

# A Coupled Inductor Dual-Input Bipolar Triple-Output Buck Converter with Sliding Mode Controller

Isac Daimary *Student Member, IEEE*  
 Department of Electrical Engineering  
 National Institute of Technology Arunachal Pradesh  
 Jote, India  
 isac.phd@nitap.ac.in

Rajib Jana *Member, IEEE*  
 Department of Electrical Engineering  
 National Institute of Technology Arunachal Pradesh  
 Jote, India  
 rajib@nitap.ac.in

BL Narasimharaju, *Senior Member, IEEE*  
 Department of Electrical Engineering  
 National Institute of Technology Warangal  
 Warangal, India  
 blnraju@nitw.ac.in

**Abstract**—This paper presents a thorough investigation into the challenges encountered by a coupled-inductor dual-input triple-output buck converter (CIDITO-BC) through small signal modelling. Time domain and frequency domain analysis of the small signal model reveals the effects of cross-coupling and cross-regulation issues. A sliding mode control (SMC) scheme is proposed to address such issues. The proposed sliding mode control strategy is customized for the CIDITO-BC's requirements, with design principles, implementation details, and discussions on advantages and limitations provided. Simulation results confirm the effectiveness of the proposed model and control strategy, showing enhanced stability, transient response, and efficiency under different scenarios. The designed SMC provide simultaneous regulation of output voltages at 3.3V, -3.3V and 6.6V and is validated by building a simulation prototype. The simulation results verify the SMC scheme which regulates the output voltages despite changes in load conditions and input voltages.

**Index Terms**—Sliding mode control, coupled inductor buck, small signal modelling, DC-DC converters.

## I. INTRODUCTION

The ever-expanding landscape of power electronics demands innovative solutions to address the evolving requirements of modern applications. This paper delves into the intricacies of a proposed dual-input triple-output buck converter, illustrated in Fig. 1 a configuration gaining prominence for its ability to efficiently manage multiple power sources and outputs. The proposed circuit, extendable to electric vehicle applications, promises to deliver bipolar power to ICs, meeting critical requirements. The dual-input triple-output configuration reduces the cost, volume of the converter and increases power density. DC-DC converters featuring negative output are crucial in various applications, including audio amplifiers, signal generators, and data transmission interfaces [1]. There exists number of literature based on negative output converters [2, 3]. In the

realm of negative output (N-O) converters, the buck-boost and Cuk converters are commonly encountered, each exhibiting a voltage conversion ratio of  $\frac{-D}{(1-D)}$ . Furthermore, flyback converters offer an alternative method for achieving negative output voltage. However, it's worth noting that employing transformers in these converters can lead to increased volume, diminished efficiency, switch voltage overshoot, and electromagnetic interference (EMI) concerns [4]. The CIDITO-BC, as proposed, possesses distinctive capabilities enabling it to deliver outputs of both negative and positive polarity.

Power converters designed with coupled inductors inherently exhibit cross-coupling and cross-regulation issues. Cross-coupling refers to the impact on the output resulting from variations in the duty cycle, while cross-regulation denotes the effect on one output due to changes in the load current of another output. This issues are generally mitigated by improving the transient response of the converter. Sliding mode control is renowned for its inherent ability to effectively handle uncertainties and disturbances, making it particularly well-suited for addressing the challenges posed by the converter's

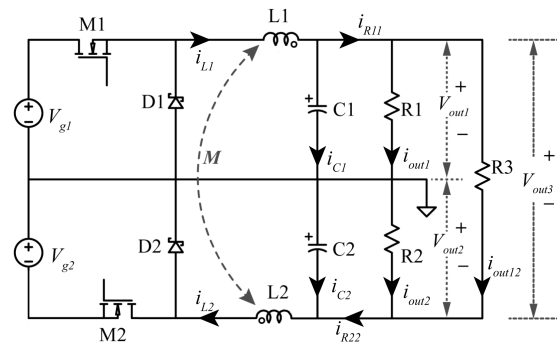


Fig. 1: Circuit diagram of the CIDITO-BC.

complex configuration.

The paper is centered on investigating the operational characteristics of the proposed CIDITO-BC in both steady-state and transient conditions. The contributions of the paper are delineated as follows:

- Small-signal modeling of the converter.
- Designing a sliding surface and hence sliding mode controller for CIDITO-BC.
- Proposed methodology is verified in LTspice and MATLAB environment.

## II. LITERATURE REVIEW

In literature, power converters based on coupled inductors have been extensively studied [5, 6]. Among these, single-input multiple-output (SIMO), specifically two output configurations have been investigated [7–9]. However, a common issue encountered in such converters is cross-coupling and cross-regulation. Various control techniques and circuit configuration have been proposed to mitigate or alleviate these effects. For instance, in [10, 11], control technique such as time multiplexing control is used, while the converter is operated in discontinuous conduction mode (DCM). However operating a converter in DCM has its own disadvantages viz. higher output ripple, reduced efficiency at light loads, limited operating range etc. In [12], a decoupled voltage mode control (VMC) technique is utilized to minimize cross-coupling and cross-regulation. Despite its effectiveness, VMC alone may not completely eliminate these effects and often requires high loop gain to achieve its objectives. However, high loop gain can lead to system instability [13], rendering this approach unsuitable for many applications. Additionally, VMC does not account for system nonlinearities, thus reducing robustness. A practical approach to mitigate the issues of cross-coupling and cross-regulation in CIDITO-BC involves enhancing the transient response of the converter. SMC are well known for their ability to handle large transient disturbances. This paper proposes the utilization of SMC in a multiple-input multiple-output buck converter, specifically to CIDITO-BC.

## III. DUAL INPUT TRIPLE OUTPUT BUCK CONVERTER

### A. Circuit operation

The circuit diagram of CIDITO-BC is depicted in Fig. 1. The circuit comprises two input voltage sources  $V_{g1}$  and  $V_{g2}$ . Switches  $M1$  and  $M2$ , along with diodes  $D1$  and  $D2$ , regulate the power flow from inputs to the outputs. The converter features three outputs:  $V_{out1}$ ,  $V_{out2}$ , and  $V_{out12}$ .

Among these,  $V_{out2}$  exhibits negative polarity, and it holds that  $V_{out12} = V_{out1} + V_{out2}$ . Additionally, for ease of derivation,  $R_{11} = R_1 || R_3$ , and  $R_{22} = R_2 || R_3$  are considered. It is confirmed that this assumption does not compromise the overall circuit operation. The output voltages  $V_{out1}$  and  $V_{out2}$  are regulated by duty cycles  $d_1$  and  $d_2$ , respectively. Notably, the circuit displays symmetry, denoted as upper-buck and lower-buck centered around the ground reference. The circuit operates in four modes: Mode-I, Mode-II, Mode-III, and Mode-IV. Fig. 2 illustrates the equivalent circuits for different operating modes. During Mode-I, both mosfet switches are active, storing energy in inductors  $L1$  and  $L2$  and capacitors  $C1$  and  $C2$ . In Mode-II, mosfet  $M2$  is turned off, leading to the discharge of capacitor  $C2$ . Mode-III involves the deactivation of mosfet  $M1$ , resulting in the discharge of capacitor  $C1$ . In Mode-IV, both switches  $M1$  and  $M2$  are off, causing both capacitors to discharge. This cyclic process of inductor magnetization and capacitor discharge recurs based on the pulse width modulation (PWM) type, determining the circuit's operating mode. A negative coupling coefficient ( $k$ ) is assumed, indicating inverse winding coupling. Assuming ideal mosfets and diodes, the derived voltage transfer ratio is expressed as:

$$V_{out1} = d_1 V_{g1}, \quad V_{out2} = -d_2 V_{g2}$$

## IV. SMALL SIGNAL ANALYSIS

To elucidate the transient performance of the converter, small-signal analysis is conducted on the CIDITO-BC, leading to the derivation of transfer functions. The analysis is carried out utilizing the state-space averaging technique [14]. The model derived is given as below:

$$\frac{d\hat{x}}{dt} = A\hat{x} + B\hat{u} \quad \hat{y} = C\hat{x} + D\hat{u} \quad (1)$$

where

$$\hat{x} = [ \tilde{i}_{L1} \quad \tilde{v}_{C1} \quad \tilde{i}_{L2} \quad \tilde{v}_{C2} ]^T$$

$$\hat{u} = [ \tilde{v}_{g1} \quad \tilde{v}_{g2} \quad \tilde{d}_1 \quad \tilde{d}_2 \quad \tilde{i}_{out1} \quad \tilde{i}_{out2} ]^T$$

$$y = [ \tilde{v}_{out1} \quad \tilde{v}_{out2} ]^T$$

$$A = \begin{bmatrix} \frac{L_2(r_{L1}+r'_1)}{L_M} & \frac{L_2 r'_1}{L_M} & \frac{M(r_{L2}+r'_2)}{L_M} & -\frac{M r'_2}{L_M} \\ \frac{r'_1}{C_1} & -\frac{r'_{11}}{C_1} & 0 & 0 \\ \frac{M(r_{L1}+r'_1)}{L_M} & -\frac{M r'_1}{L_M} & \frac{L_1(r_{L2}+r'_2)}{L_M} & \frac{L_1 r'_2}{L_M} \\ 0 & 0 & \frac{r'_2}{C_2} & -\frac{r'_{22}}{C_2} \end{bmatrix}$$

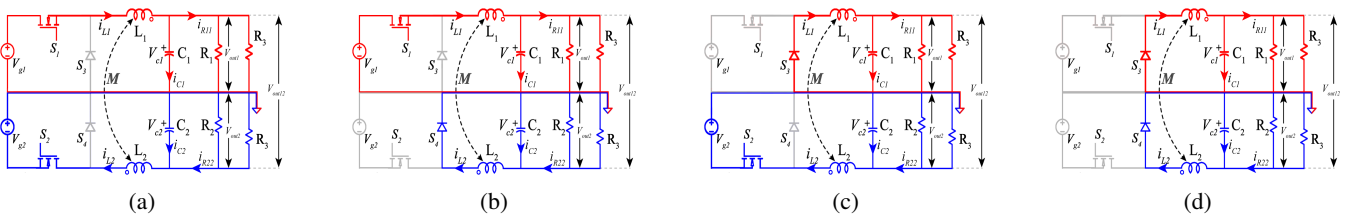


Fig. 2: Circuit operation: (a) Mode-I (b) Mode-II (c) Mode-III and (d) Mode-IV

$$B = \begin{bmatrix} -\frac{L_2 d_1}{L_M} & \frac{M d_2}{L_M} & -\frac{L_2 V_{g1}}{L_M} & \frac{M V_{g2}}{L_M} & 0 & 0 \\ 0 & 0 & 0 & 0 & -\frac{r''_1}{C_1} & 0 \\ \frac{M d_1}{L_M} & -\frac{L_1 d_2}{L_M} & \frac{M V_{g1}}{L_M} & -\frac{L_1 V_{g2}}{L_M} & 0 & 0 \\ 0 & 0 & 0 & 0 & 0 & -\frac{r''_2}{C_2} \end{bmatrix}$$

$$C = \begin{bmatrix} r'_1 & r'_1 & 0 & 0 \\ 0 & 0 & -r'_2 & -r'_2 \end{bmatrix}$$

$$D = \begin{bmatrix} 0 & 0 & 0 & 0 & -r'_1 & 0 \\ 0 & 0 & 0 & 0 & 0 & r'_2 \end{bmatrix}$$

and  $L_M = M^2 - L_1 L_2$ ,  $r'_1 = \frac{R_{11} r_{c1}}{R_{11} + r_{c1}}$ ,  $r''_1 = \frac{R_{11}}{R_{11} + r_{c1}}$ ,  $r'_{11} = \frac{1}{(R_{11} + r_{c1})}$ ,  $r'_2 = \frac{R_{22} r_{c2}}{R_{22} + r_{c2}}$ ,  $r''_2 = \frac{R_{22}}{R_{22} + r_{c2}}$ ,  $r'_{22} = \frac{1}{(R_{22} + r_{c2})}$  and  $M = k\sqrt{L_1 L_2}$ . The effective series resistances (ESR) of capacitor  $C_1$  and  $C_2$  are considered as  $r_{c1}$  and  $r_{c2}$  respectively. Taking the Laplace transform of equation (1), the transfer function of the system is  $\hat{Y}(s) = (C(sI - A)^{-1}B + D)\hat{U}(s)$  and is written in matrix form as

$$\begin{bmatrix} \tilde{v}_{out1} \\ \tilde{v}_{out2} \end{bmatrix} = \begin{bmatrix} G_{vg11} & G_{vg12} \\ G_{vg21} & G_{vg22} \end{bmatrix} \begin{bmatrix} \tilde{v}_{g1} \\ \tilde{v}_{g2} \end{bmatrix} + \begin{bmatrix} G_{vd11} & G_{vd12} \\ G_{vd21} & G_{vd22} \end{bmatrix} \begin{bmatrix} \tilde{d}_1 \\ \tilde{d}_2 \end{bmatrix} + \begin{bmatrix} Z_{out11} & Z_{out12} \\ Z_{out21} & Z_{out22} \end{bmatrix} \begin{bmatrix} \tilde{i}_{out1} \\ \tilde{i}_{out2} \end{bmatrix} \quad (2)$$

Fig. 3 represents the block diagram of the small-signal model.

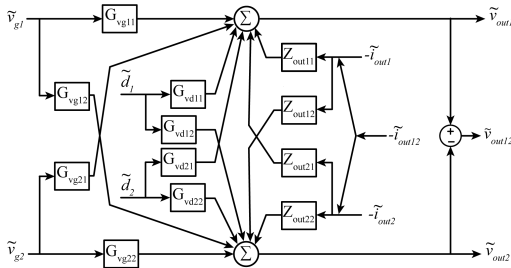


Fig. 3: Small signal model.

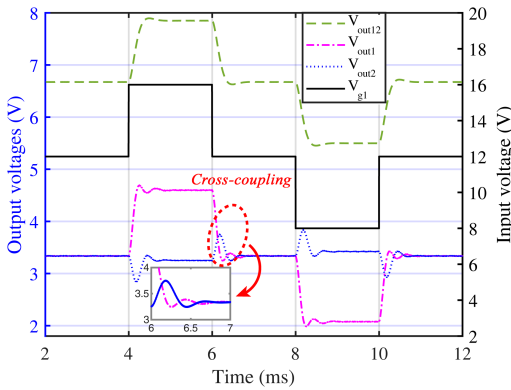


Fig. 4: Output voltage response for step change in input voltage ( $V_{g1}$ ) in port-I.

While examining the step responses of the transfer function

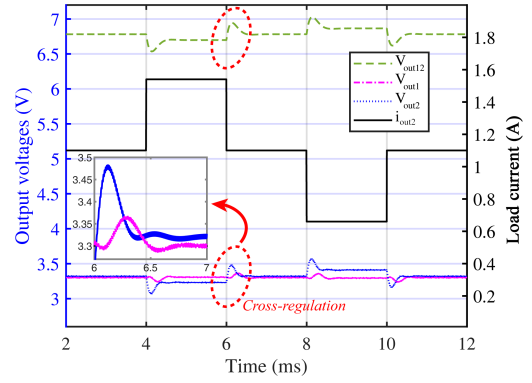


Fig. 5: Output voltage response for step change in load current ( $i_{out2}$ ) at output port-II

described in equation (2), observations were made regarding the impacts of cross-coupling and cross-regulation. The simulation is done in MATLAB2021a from the parameters given in Table I. Fig. 4 illustrates the cross-coupling phenomenon, where a step change in the input voltage ( $V_{g1}$ ) at input port-I affects the output of port-II and port-III. and Fig. 5 illustrates the cross-regulation phenomenon, a step change in the load current ( $i_{out2}$ ) at output port-II affects the output of port-I and port-III. The frequency domain response is also observed and presented in Fig. 6. From figure it is observed that the self transfer function ( $G_{vd22}, Z_{out22}$ ) is greater than that of cross transfer function, ( $G_{vd21}, Z_{out12}$ ). The response of the small-signal analytical model is compared with that of the circuit model, revealing a close resemblance between the two. The circuit model is simulated in LTspice. LTspice is a versatile software tool extensively used in the design of DC-DC converters [15].

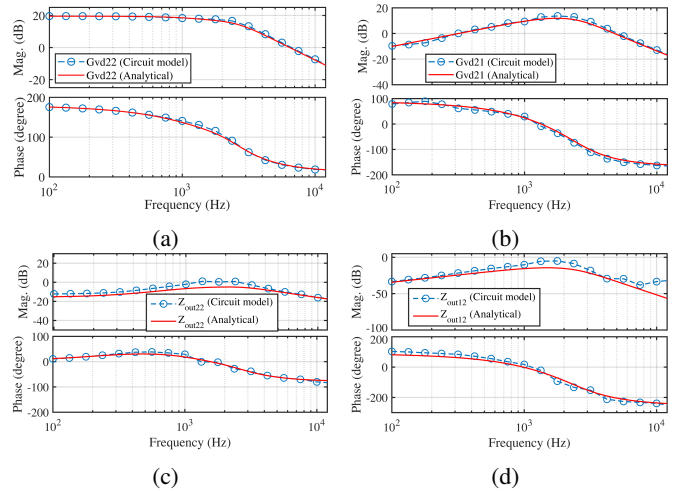


Fig. 6: Various transfer functions: (a)  $G_{vd22}$  (b)  $G_{vd21}$  (c)  $Z_{out22}$  (d)  $Z_{out12}$

## V. ON DESIGNING SLIDING MODE CONTROLLER

SMCs are renowned for their robustness in managing uncertainties and nonlinearities within dynamical systems. Fun-

damental to SMCs is the establishment of a sliding surface within the state space, guiding system trajectories to this surface and ensuring robust performance [16, 17]. Despite the challenge of chattering—a phenomenon of high-frequency oscillations—the benefits of SMCs are significant. In this paper the boundary layer condition and sliding surface design for CIDITO-BC has been briefly presented. The voltage error  $x_1$  and the voltage error dynamics (or the rate of change of voltage error)  $x_2$  under continuous conduction mode (CCM) of operation can be expressed as

$$x_1 = V_{ref1} - \beta_1 V_{out1} \quad (3)$$

$$x_2 = \dot{x}_1 = -\beta_1 \frac{dV_{out1}}{dt} \quad (4)$$

Since,  $i_{L1} = i_{C1} + i_{R11}$ , equation (4) can be written as

$$= \frac{\beta_1}{C_1} \left( \frac{V_{out1}}{R_{11} || R_{12}} - \int \frac{MV_{g2}u_2 - L_2V_{g1}u_1 + MV_{o2} + L_2V_{o1}}{M^2 - L_1L_2} dt \right) \quad (5)$$

Where the equation for inductor currents  $i_{L1}$  and  $i_{L2}$  is

$$i_{L1} = \int \frac{MV_{g2}u_2 - L_2V_{g1}u_1 + MV_{o2} + L_2V_{o1}}{M^2 - L_1L_2} dt \quad (6)$$

$$i_{L2} = \int \frac{MV_{g1}u_1 - L_1V_{g2}u_2 - MV_{o1} - L_1V_{o2}}{M^2 - L_1L_2} dt \quad (7)$$

Now taking derivative of Equation (5) and with some algebraic manipulations

$$\begin{aligned} \dot{x}_2 = & \frac{L_2}{C_1(M^2 - L_1L_2)}x_1 - \frac{1}{C_1R_{11}}x_2 + \frac{\beta_1M}{\beta_2C_1(M^2 - L_1L_2)}x_3 \\ & + \frac{\beta_1L_2V_{g1}}{C_1(M^2 - L_1L_2)}u_1 - \frac{\beta_1MV_{g2}}{C_1(M^2 - L_1L_2)}u_2 \\ & - \frac{L_2V_{ref1}}{C_1(M^2 - L_1L_2)} - \frac{\beta_1MV_{ref2}}{C_1\beta_2(M^2 - L_1L_2)} \end{aligned} \quad (8)$$

The  $\dot{x}_1$  and  $\dot{x}_2$  are associated with input port-I to output port-I (upper buck in Fig. 1). Similar steps with taking account of equation (7) can be applied to input port-II to output port-II. In this case,  $x_3 = V_{ref2} - \beta_2 V_{out2}$  and  $x_4 = \dot{x}_3 = -\beta_2 \frac{dV_{out2}}{dt}$  is considered.

$$\begin{aligned} \dot{x}_4 = & \frac{\beta_2M}{\beta_1C_2(M^2 - L_1L_2)}x_1 + \frac{L_1}{C_2(M^2 - L_1L_2)}x_3 - \frac{1}{C_2R_{22}}x_4 \\ & + \frac{\beta_2MV_{g1}}{C_2(M^2 - L_1L_2)}u_1 - \frac{\beta_2L_1V_{g2}}{C_2(M^2 - L_1L_2)}u_2 \\ & - \frac{\beta_2MV_{ref1}}{\beta_1C_2(M^2 - L_1L_2)} - \frac{L_1V_{ref2}}{C_2(M^2 - L_1L_2)} \end{aligned} \quad (9)$$

The equations obtained so far can be arranged in matrix form as shown below:

$$\begin{aligned} \begin{bmatrix} \dot{x}_1 \\ \dot{x}_2 \\ \dot{x}_3 \\ \dot{x}_4 \end{bmatrix} = & \begin{bmatrix} 0 & 1 & 0 & 0 \\ \frac{L_2}{C_1L_M} & -\frac{1}{C_1R_{11}} & \frac{\beta_1M}{\beta_2C_1L_M} & 0 \\ 0 & 0 & 0 & 1 \\ \frac{\beta_2M}{\beta_1C_2L_M} & 0 & \frac{L_1}{C_2L_M} & -\frac{1}{C_2R_{22}} \end{bmatrix} \begin{bmatrix} x_1 \\ x_2 \\ x_3 \\ x_4 \end{bmatrix} \\ & + \begin{bmatrix} 0 & 0 \\ \frac{\beta_1L_2V_{g1}}{C_1L_M} & -\frac{\beta_1MV_{g2}}{C_1L_M} \\ 0 & 0 \\ \frac{\beta_2MV_{g1}}{C_2L_M} & -\frac{\beta_2L_1V_{g2}}{C_2L_M} \end{bmatrix} \begin{bmatrix} u_1 \\ u_2 \end{bmatrix} + \begin{bmatrix} 0 \\ -\frac{L_2V_{ref1}}{\beta_1C_2L_M} - \frac{\beta_1MV_{ref2}}{\beta_2C_1L_M} \\ 0 \\ -\frac{\beta_2MV_{ref1}}{\beta_1C_2L_M} - \frac{L_1V_{ref2}}{C_2L_M} \end{bmatrix} \end{aligned} \quad (10)$$

### A. Controller's model

The sliding mode voltage controller adopted in this study controls the state variables  $x_1$ ,  $x_2$ ,  $x_3$  and  $x_4$ . Hence the switching state  $u_1$  and  $u_2$  can be determined from the control parameters using the switching function as:

$$u_1 = \begin{cases} 1 & \text{when } S_1 > h_1 \\ 0 & \text{when } S_1 < -h_1 \\ \text{unchanged} & \text{otherwise} \end{cases} \quad (11)$$

$$u_2 = \begin{cases} 1 & \text{when } S_2 > h_2 \\ 0 & \text{when } S_2 < -h_2 \\ \text{unchanged} & \text{otherwise} \end{cases} \quad (12)$$

where the control signals  $S_1$  and  $S_2$  are given as

$$S_1 = \frac{C_1}{\beta_1}\alpha_1x_1 + \frac{C_1}{\beta_1}x_2 \text{ and } S_2 = \frac{C_2}{\beta_2}\alpha_2x_3 + \frac{C_2}{\beta_2}\alpha_2x_4 \quad (13)$$

In matrix form  $S_1$  and  $S_2$ , in the form  $S = Jx$ , are given as

$$S_1 = \begin{bmatrix} \frac{C_1}{\beta_1}\alpha_1 & \frac{C_1}{\beta_1} & 0 & 0 \end{bmatrix} \begin{bmatrix} x_1 \\ x_2 \\ x_3 \\ x_4 \end{bmatrix} \quad (14)$$

$$S_2 = \begin{bmatrix} 0 & 0 & \frac{C_2}{\beta_2}\alpha_2 & \frac{C_2}{\beta_2} \end{bmatrix} \begin{bmatrix} x_1 \\ x_2 \\ x_3 \\ x_4 \end{bmatrix}. \quad (15)$$

For stability

$$\dot{S}_1 = \begin{cases} J_1\dot{x} < 0 & \text{for } 0 < S_1 < \xi_1 \\ J_1\dot{x} > 0 & \text{for } -\xi_1 < S_1 < 0 \end{cases} \quad (16)$$

$$\dot{S}_2 = \begin{cases} J_2\dot{x} < 0 & \text{for } -\xi_2 < S_2 < 0 \\ J_2\dot{x} > 0 & \text{for } 0 < S_2 < \xi_2 \end{cases} \quad (17)$$

The condition for sliding mode control to exist is

$$\lambda_1 = J_1 \cdot \dot{x} \quad \text{and} \quad \lambda_2 = J_2 \cdot \dot{x} \quad (18)$$

From equation (10) and equation (14, 15), the condition for  $\alpha_1$  and  $\alpha_2$  can be determined

$$\alpha_1 < \begin{cases} -\frac{L_2V_{g1}}{L_M|i_{c1}|} - \left( \frac{MV_{out2} - L_2V_{out1}}{L_M|i_{c1}|} - \frac{MV_{g2}u_2}{L_M|i_{c1}|} \right) + \frac{1}{R_{11}C_1}, \\ \text{for } V_{g1(\min)} > -k\sqrt{\frac{L_1}{L_2}}V_{out1(\max)} + V_{out2(\max)}. \\ \frac{MV_{out2} - L_2V_{out1}}{L_M|i_{c1}|} - \frac{MV_{g2}u_2}{L_M|i_{c1}|} + \frac{1}{R_{11}C_1}, & \text{otherwise.} \end{cases} \quad (19)$$

$$\alpha_2 < \begin{cases} -\frac{L_1V_{g2}}{L_M|i_{c2}|} - \left( \frac{MV_{out1} - L_1V_{out2}}{L_M|i_{c2}|} - \frac{MV_{g1}u_1}{L_M|i_{c2}|} \right) - \frac{1}{R_{22}C_2}, \\ \text{for } V_{g2(\min)} > -k\sqrt{\frac{L_2}{L_1}}V_{out2(\max)} + V_{out1(\max)}. \\ \frac{MV_{out1} - L_1V_{out2}}{L_M|i_{c2}|} - \frac{MV_{g1}u_1}{L_M|i_{c2}|} - \frac{1}{R_{22}C_2}, & \text{otherwise.} \end{cases} \quad (20)$$

The selection of  $\alpha_1$  and  $\alpha_2$  plays a pivotal role in governing the regions of existence and influencing the dynamic response of the system [18]. Therefore, to uphold a favorable region of existence and dynamic response,  $\alpha_1$  and  $\alpha_2$  are chosen as  $\alpha_1 = \frac{1}{R_{11}C_1}$ ,  $\alpha_2 = \frac{1}{R_{22}C_2}$

## B. Switch stress

The voltage stress in the two MOSFET switches is as follows:

- Voltage stress in switch 1 ( $M_1$ ):  $V_{g1}$
- Voltage stress in switch 2 ( $M_2$ ):  $V_{g2}$

## VI. SIMULATION MODEL

To assess the effectiveness of the proposed controller, a circuit model simulation is conducted using LTspice. The Schmitt trigger in Fig. 7 is utilized to generate a control signals ( $u_1, u_2$ ) dependent on  $S_1$  and  $S_2$ . The following parameters of the SMC are employed for simulation:

- $\beta_1, \beta_2 = 0.275$ ,  $V_{ref1} = 0.9075$ ,  $V_{ref2} = -0.9075$ .

Due to the inherent chattering issue in SMC, hysteresis modulators are implemented with control over the hysteresis band ' $h_1, h_2$ '. In this case Schmitt trigger are used as the hysteresis modulator and the hysteresis band can be adjusted by the resistor ratio  $\frac{R_{SM2}}{R_{SM1}}$  in Fig. 7a and  $\frac{R_{SC2}}{R_{SC1}}$  in Fig. 7b. Another way to do it is by adjusting the supply voltages  $\frac{V_{C1+}}{V_{C1-}}$  and  $\frac{V_{C2+}}{V_{C2-}}$ . In this work, for easy implementation, latter option is opted for. The expression for hysteresis band are given as:

$$h_1 = \frac{R_{SM1}}{R_{SM2}} (V_{C1+} - V_{C1-}), \quad h_2 = \frac{R_{SC1}}{R_{SC2}} (V_{C2+} - V_{C2-})$$

In this work, for the operating frequency of 255 kHz,  $h_1$  and  $h_2$  is 0.2. Some other parameters are  $R_{SM1} = R_{SC1} = 2k\Omega$ ,  $R_{SM2} = R_{SC2} = 100k\Omega$ . Also, during steady state  $V_{C1+} = V_{C2+} = 5V$  and  $V_{C1-} = V_{C2-} = -5V$ . The derived expression for  $S_1$  and  $S_2$  in Fig. 7 are :

$$S_1 = \frac{i_{B11}}{\beta_1 V_{out1}} (V_{ref1} - \beta_1 V_{out1}) - i_{C1}$$

$$S_2 = \frac{i_{B22}}{\beta_2 V_{out2}} (V_{ref2} - \beta_2 V_{out2}) - i_{C2}$$

The parameter  $S_1$  and  $S_2$  are used to generate control signal  $u_1$  and  $u_2$ . Further, the driver ICs uses  $u_1$  and  $u_2$  to drive mosfet M1 and M2 respectively.

TABLE I  
Design parameters of CIDITO-BC

Sl. No.	Converter parameter	Value
1	Input nominal voltage 1 ( $V_{g1}$ )	12V
2	Input nominal voltage 2 ( $V_{g2}$ )	12V
3	Output voltage 1 ( $V_{out1}$ )	3.3V
4	Output voltage 2 ( $V_{out2}$ )	-3.3V
5	Output voltage 3 ( $V_{out12}$ )	6.6V
6	Load resistor of output 1 ( $R1$ )	2 $\Omega$
7	Load resistor of output 2 ( $R2$ )	2 $\Omega$
8	Load resistor of output 3 ( $R12$ )	3 $\Omega$
9	Primary Inductance of coupled inductor ( $L_1$ )	100 $\mu H$
10	Secondary Inductance of coupled inductor ( $L_2$ )	100 $\mu H$
11	Mutual Inductance ( $M$ )	50 $\mu H$
12	DCR of both the inductor ( $r_{dc}$ )	0.12 $\Omega$
13	Capacitor of output 1 ( $C_1$ )	100 $\mu F$
14	Capacitor of output 2 ( $C_2$ )	100 $\mu F$
15	ESR of both the Capacitor ( $r_{c1}, r_{c2}$ )	0.012 $\Omega$

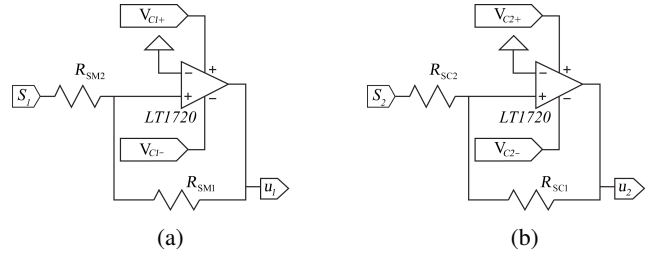


Fig. 7: Schematic circuit diagram of a Schmitt trigger to generate control signals  $u_1$  and  $u_2$ : (a) for upper buck (b) for lower buck.

## VII. SIMULATION RESULTS

### A. Audio-susceptibility test

To initiate testing of the controller, a series of experiments are conducted. In Fig. 8, a step change in input voltage is depicted at input port-I. It is evident from the graph that the controller effectively manages line disturbances, resulting in the elimination of transients in output voltages  $V_{out2}$  and  $V_{out12}$ . Also the output voltage  $V_{out1}$  remain regulated.

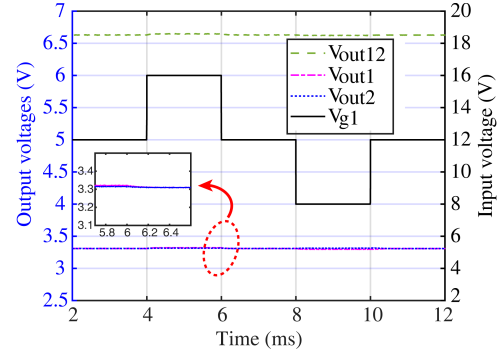


Fig. 8: A sudden input voltage change at input Port-I ( $V_{g1}$ ). Responses in output voltages at Port-I ( $V_{out1}$ ), Port-II ( $V_{out2}$ ), and Port-III ( $V_{out12}$ ).

### B. Self-regulation and cross-regulation test

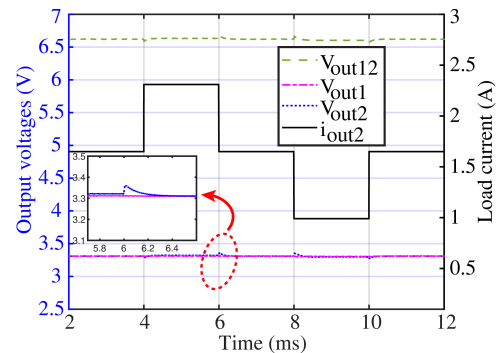


Fig. 9: A step load current change at output Port-II ( $i_{out2}$ ). Responses in output voltages at Port-I ( $V_{out1}$ ), Port-II ( $V_{out2}$ ), and Port-III ( $V_{out12}$ ).

Likewise, similar observations are noted during load step changes, as illustrated in Fig. 9 and Fig. 10. Despite a step

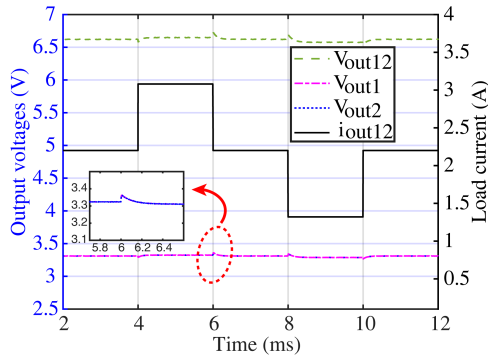


Fig. 10: A step load current change at output Port-III ( $i_{out12}$ ). Responses in output voltages at Port-I ( $V_{out1}$ ), Port-II ( $V_{out2}$ ), and Port-III ( $V_{out12}$ ).

change in output load current at port-II and port-III, the robustness of the controller mitigates its impact on output voltages  $V_{out1}$ ,  $V_{out2}$  and  $V_{out12}$ . These shows the improvement in cross-regulation. At the same time, the output voltage  $V_{out1}$  remain regulated, indicating improvement in self-regulation. Fig. 11 shows the waveform of PWM1 and PWM2 at a frequency of 255 kHz.

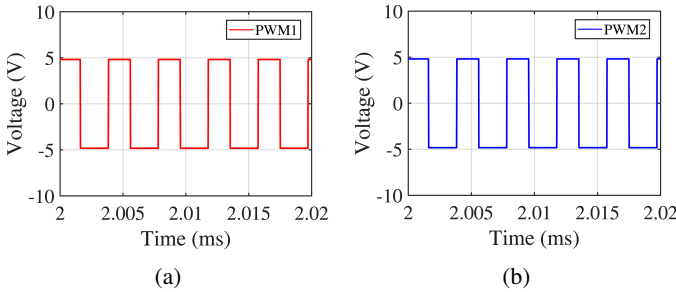


Fig. 11: Waveforms: (a) PWM1 (b) PWM2

## VIII. CONCLUSION

In conclusion, this paper has presented the modeling of the CIDITO-BC using small signal analysis, accompanied by the development of a sliding mode controller to mitigate cross-coupling and cross-regulation issues. Through simulation validation, promising enhancements in stability and transient response have been demonstrated. The integration of the proposed sliding mode controller effectively regulates output voltages amidst step changes in input voltages and load currents, thus addressing the demand for efficient power electronic systems in modern applications. The comprehensive simulation results, supported by mathematical derivations, signify a significant contribution to the field of power electronics. While certain derivations have been intentionally preserved for future investigations to maintain focus on the primary objectives of this study, they pave the way for continued depth and exploration within this domain.

## REFERENCES

- [1] S. Ding and F. Wang, "A new negative output buck-boost converter with wide conversion ratio," *IEEE Transactions on Industrial Electronics*, vol. 64, no. 12, pp. 9322–9333, 2017.
- [2] K. I. Hwu and Y. T. Yau, "Soft switching of negative-output ky buck converter;" in *2009 Twenty-Fourth Annual IEEE Applied Power Electronics Conference and Exposition*, 2009, pp. 1053–1060.
- [3] J. Li and J. Liu, "A negative-output high quadratic conversion ratio dc-dc converter with dual working modes," *IEEE Transactions on Power Electronics*, vol. 34, no. 6, pp. 5563–5578, 2019.
- [4] Y. Tang, T. Wang, and Y. He, "A switched-capacitor-based active-network converter with high voltage gain," *IEEE Transactions on Power Electronics*, vol. 29, no. 6, pp. 2959–2968, 2014.
- [5] G. Zhu, B. A. McDonald, and K. Wang, "Modeling and analysis of coupled inductors in power converters," *IEEE Transactions on Power Electronics*, vol. 26, no. 5, pp. 1355–1363, 2011.
- [6] H. N. Nagaraja, D. Kastha, and A. Petra, "Design principles of a symmetrically coupled inductor structure for multiphase synchronous buck converters," *IEEE Transactions on Industrial Electronics*, vol. 58, no. 3, pp. 988–997, 2011.
- [7] Y. Wang, J. Xu, and G. Yin, "Cross-regulation suppression and stability analysis of capacitor current ripple controlled side ccm buck converter;" *IEEE Transactions on Industrial Electronics*, vol. 66, no. 3, pp. 1770–1780, 2019.
- [8] G. Nayak and S. Nath, "Decoupled average current control of coupled inductor single-input dual-output buck converter," *IEEE Journal of Emerging and Selected Topics in Industrial Electronics*, vol. 1, no. 2, pp. 152–161, 2020.
- [9] P. Patra, J. Ghosh, and A. Patra, "Control scheme for reduced cross-regulation in single-inductor multiple-output dc-dc converters," *IEEE Transactions on Industrial Electronics*, vol. 60, no. 11, pp. 5095–5104, 2013.
- [10] W. Huang, J. A. Abu Qahouq, Z. Dang, and C. Johnson, "Dcm control scheme for single-inductor multiple-output dc-dc converter with no cross-regulation," in *2015 IEEE Applied Power Electronics Conference and Exposition (APEC)*, 2015, pp. 385–391.
- [11] H. Chen, Y. Zhang, and D. Ma, "A simo parallel-string driver ic for dimmable led backlighting with local bus voltage optimization and single time-shared regulation loop," *IEEE Transactions on Power Electronics*, vol. 27, no. 1, pp. 452–462, 2012.
- [12] G. Nayak and S. Nath, "Decoupled voltage-mode control of coupled inductor single-input dual-output buck converter," *IEEE Transactions on Industry Applications*, vol. 56, no. 4, pp. 4040–4050, 2020.
- [13] X. Ruan, C. Xiong, X. Li, X. Xiong, Q. Jin, M. Sha, and C. K. Tse, "Reconsideration of loop gain and its measurement in dc-dc converters," *IEEE Transactions on Power Electronics*, vol. 34, no. 7, pp. 6906–6921, 2019.
- [14] R. D. Middlebrook and S. Cuk, "A general unified approach to modelling switching-converter power stages," in *1976 IEEE Power Electronics Specialists Conference*, 1976, pp. 18–34.
- [15] I. Daimary and R. Jana, "Design and implementation of type-iii controller in voltage-mode-controlled inverting buck-boost converter using Ispice," in *2023 IEEE 3rd International Conference on Sustainable Energy and Future Electric Transportation (SEFET)*, 2023, pp. 1–5.
- [16] H. Komurcugil, S. Biricik, S. Bayhan, and Z. Zhang, "Sliding mode control: Overview of its applications in power converters," *IEEE Industrial Electronics Magazine*, vol. 15, no. 1, pp. 40–49, 2021.
- [17] Y. Zhao, W. Qiao, and D. Ha, "A sliding-mode duty-ratio controller for dc/dc buck converters with constant power loads," *IEEE Transactions on Industry Applications*, vol. 50, no. 2, pp. 1448–1458, 2014.
- [18] S.-C. Tan, Y. Lai, M. Cheung, and C. Tse, "On the practical design of a sliding mode voltage controlled buck converter," *IEEE Transactions on Power Electronics*, vol. 20, no. 2, pp. 425–437, 2005.